Nature Environment and Pollution Technology
An International Quarterly Scientific Journal

p-ISSN: 0972-6268
(Print copies up to 2016)
e-ISSN: 2395-3454

Vol. 22 | No. 3 | pp. 1547-1554 | 2023

Original Research Paper

https://doi.org/10.46488/NEPT.2023.v22i03.040

Open Access Journal

Study on the Experimental Conditions of Adsorption of Lanthanum (III) on Boron Nitride Nanosheets

C. Fu*, Y. He*, C. Yang*, J. He*, L. Sun*, G. Sheng*, X. Zhang, L. Wang*†, L. Li* and W. Linghu***

*School of Chemistry and Chemical Engineering, Department of Zhejiang Engineering Research Center of Fat-soluble Vitamin, Shaoxing University, Zhejiang 312000, P. R. China

**Department of International Education, Beijing University of Chemical Technology, Beijing 100029, P. R. China

†Corresponding authors: Linxia Wang; wlxsyx@163.com

Nat. Env. & Poll. Tech.
Website: www.neptjournal.com

Received: 14-02-2023
Revised: 14-04-2023
Accepted: 18-04-2023

Key Words:
Boron nitride
Adsorption
Lanthanum(III)
Nanosheets

ABSTRACT

This paper investigated the adsorption properties of boron nitride materials for La(III), and the possible action mechanism was put forward based on experiments. Then the boron nitride materials were characterized by SEM, TEM, XRD, and FT-IR before and after adsorption. In addition, the effects of pH, the amount of adsorbent, the concentration of La(III) solution, and adsorption time on the adsorption efficiency were also investigated. It is found that under a certain amount of adsorbent when the pH is 7.0 and the concentration of La(III) is 40 $mg.L^{-1}$, the adsorption ability of La(III) is the best. The maximum adsorption capacity is 201.45 $mg.g^{-1}$. The adsorption kinetic data are in good agreement with the pseudo-second-order and intra-particle diffusion models. These results show that boron nitride has a good application prospect for removing and recovering La(III) in water and has a certain practical application value.

INTRODUCTION

Due to their excellent properties, rare earth elements are widely used in metallurgy, petrochemicals, glass, ceramics, aerospace, and other fields. Therefore, rare earth elements are also known as "industrial vitamins." In recent years, with the continuous development of science and technology, the demand for rare earth elements keeps rising. Lanthanum, one of the most common rare earth elements (Wu et al. 2011), is usually used in synthesizing superalloys and preparing catalysts (Sert et al. 2008). As one of the most used rare earth elements, lanthanum also causes some pollution to the ecological environment. For example, manufacturing various industrial materials and using agricultural rare earth fertilizers will lead to soil pollution (Shen et al. 2014).

Moreover, studies have shown that rare earth minerals will produce various kinds of pollution during processing, such as harmful nitrogen and chloride produced by hydrometallurgy and harmful gases such as chloroform VOCs produced by high temperatures of pyrometallurgy. Rare earth elements will induce cardiovascular diseases in the human respiratory and nervous systems (Shin et al. 2019). Lanthanum is also very harmful to the human body. Studies have shown that lanthanum may cause nervous system disorders and accumulate in bones, kidneys, spleen, and other organs (Zarros et al. 2013, Chen & Zhu 2008, Wu et al. 2005, Liu et al. 2010) and has potential effects on the immune system (Cheng et al. 2014).

To reduce the pollution caused by lanthanum and other heavy metal elements to the environment, scientific researchers have used various treatment methods. Common treatment methods include biological methods, physical-chemical methods, and so on. For example, Du et al. (2020) concluded that planting water hyacinth can effectively enrich heavy metal elements through experiments. In this case, heavy metal ions are fixed in plant roots through the water absorption of plant roots, thus playing a role of enrichment. Physical chemistry mainly includes the chemical adsorption method. At present, the chemical method is the most commonly used chemical fixation method, such as the Zhen study group, through the use of inorganic amine hydrazine hydrate and sulfur dioxide synthesis of a new collector, produced a better removal effect on metal ions (Zhen et al. 2012). In recent years, more and more researchers have explored the recovery effect of different adsorbents on lanthanum due to the high recovery rate and low cost of the adsorption method. For example, Kusrini et al. (2018) used pectin in durian peel to study the adsorption of lanthanum, and the adsorption amount was 41.2 $mg.g^{-1}$. In recent years, boron nitride has been widely used in hydrogen storage (Lale

et al. 2018), electrical breakdown (Zhi et al. 2010), and other fields because of its special properties. In addition to the above applications, some researchers have used boron nitride in adsorption. For example, Liu et al. (2018) carried out adsorption research on Cu^{2+}, Pb^{2+}, Zn^{2+}, and Cr^{3+} and found that they all had good adsorption effects, and the adsorption kinetics were all in line with the pseudo-second-order model.

Based on the above facts and analysis, this paper will study the following three aspects: First, the two-step synthesis method is used to prepare boron nitride, and the prepared material is characterized by SEM-EDS, TEM, and XRD analysis; Secondly, the adsorbent of boron nitride was used to explore the adsorption performance of boron nitride on La(III), and the reaction conditions were optimized to explore the adsorption mechanism.

MATERIALS AND METHODS

Experimental Reagents and Materials

Lanthanum nitrate, hydrochloric acid, and sodium hydroxide were provided by Shanghai Lingfeng Chemical Reagent Co., Ltd. Sulfamic acid, hydroxylamine hydrochloride, arsine azo III, citric acid, disodium hydrogen phosphate, melamine, and boric acid were provided by Shanghai Aladdin Biochemical Science and Education Co., Ltd. The purity of the reagents was all analytical grade, and the deionized water was self-made. The components of the prepared reducing agent are hydroxylamine hydrochloride and sulfamic acid, and the components of the buffer solution are citric acid and disodium hydrogen phosphate.

Experimental Equipment

The ultrasonic cleaning machine (KQ5200DA) was produced by Kunshan Ultrasonic Instrument Co., Ltd., the UV-Vis Spectrophotometer (SP-756P) was produced by Shanghai Spectrum Instrument Co., Ltd., and the vacuum drying oven (DZF-6020) was produced by Shanghai Jinghong Experimental Equipment Co., Ltd., pH meter (Five Easy plus) and electronic balance (AL204) are produced by METTLER TOLEDO (Shanghai) Co., Ltd., using the muffle furnace (KSL-1700) produced by Hefei Kejing Material Technology Co., Ltd. The pipette (7010101017) was produced by Dalong Xingchuang Experimental Instrument (Beijing) Co., Ltd., and the desktop low-temperature constant temperature shaking shaker was the IKA KS4000i control shaker produced in Germany.

Preparation of Boron Nitride Adsorbent

The research teams (Li et al. 2013, Li et al. 2020a) have detailedly explored the preparation method of boron nitride (BN). Based on this team, this experiment adopted a two-step synthesis method to prepare BN. The specific steps were: Melamine and boric acid were evenly mixed uniformly in a molar ratio of 1:2, then roasted in a tubular furnace and heated to 1100 at a certain speed, held for 1h, and then cooled to room temperature naturally to prepare BN material.

Static Adsorption Experiment

The analytical balance was used to measure 2.3392 g La $(NO_3)_3$ dissolved in deionized water and transferred to a 1000 mL volumetric bottle. Water was added for constant volume to obtain 1000 ppm La(III) solution. Several 150 mL reaction bottles were selected, and La(III) was quantitatively removed by pipetting gun. The solution was put into the reaction bottle, and deionized water was added to adjust the total volume of the solution to 100 mL. Before the adsorption experiment, 0.1 $mol{\cdot}L^{-1}$ HCl and 0.1 $mol.L^{-1}$ NaOH were used, respectively, to adjust the initial pH value of the solution. In the static adsorption experiment, 100 mL of La(III) with different initial concentrations was adjusted to explore the influence of La(III) solution with different concentrations on the adsorption performance of BN. The initial pH of the solution was 6.0. After the quantitative BN was added, the reaction bottle was placed in the ultrasonic cleaning machine for 30min ultrasonic treatments. After the ultrasound, the reaction bottle was transferred to the bench low-temperature constant temperature oscillating shaking bed for 24h to ensure the adsorption balance. To explore the influence of different amounts of adsorbent on adsorption properties, the La(III) solution was set at 50 $mg{\cdot}L^{-1}$, and the BN adsorbent dosage was set at 10, 15, 20, 25, 30, and 35 mg. Experimental studies were carried out for adsorption kinetics using 20 mg BN and La(III) solutions of 30 and 40 $mg{\cdot}L^{-1}$ at an initial pH of 7.0. The equilibrium solution was filtered through a 0.22-μm polyether sulfone membrane filter, and the solid and aqueous solutions were separated for 1 mL. The clear liquid was placed in the colorimetric tube, and 1mL reducing agent, 5 mL buffer solution, and 1 mL color developing agent were added. The absorbance was measured by SP-756P UV-visible spectrophotometer at constant volume.

Data Processing of Adsorption Experiments

The adsorption capacity of BN can be expressed by the adsorption capacity (q_e). The adsorption capacity is the amount of La(III) adsorbed per unit weight of BN. The relevant parameters are calculated by the formula (1-2):

$$q_t = \frac{C_0 - C_t}{m} V \quad \ldots(1)$$

$$q_e = \frac{C_0 - C_e}{m} V \quad \ldots(2)$$

The adsorption capacity at equilibrium and at any time t is expressed as q_e and q_t (mg·g^{-1}). C_0 is the initial concentration of La(III) solution before adsorption (mg·L^{-1}); C_e is the concentration of La(III) solution after adsorption equilibrium, V is the volume of the solution, and m is the mass of the adsorbent.

In this study, the pseudo-first-order model, pseudo-second-order model (Wang et al. 2021), Elovich model (Wu et al. 2009), and intra-particle diffusion model (Li et al. 2020b) were used to fit the kinetic data. The calculation formulas of the relevant parameters are as follows.

Pseudo-first-order model:

$$ln\,(q_e - q_t) = lnq_e - k_1 t \quad \ldots(3)$$

pseudo-second-order model:

$$\frac{t}{q_t} = \frac{1}{k_2 q_e^2} + \frac{t}{q_e} \quad \ldots(4)$$

Elovich model:

$$q_t = \frac{1}{\beta} \cdot ln\alpha\beta + \frac{1}{\beta} \cdot lnt \quad \ldots(5)$$

intra-particle diffusion model:

$$q_t = K_d \times t^{1/2} + I \quad \ldots(6)$$

k_1(min^{-1}) is the pseudo-first-order kinetic adsorption rate constant. The pseudo-second-order kinetic adsorption rate constant is k_2 (g·mg^{-1} min^{-1}), α(mg·g^{-1} min) and β(g·mg^{-1}) represent the initial adsorption rate constant and desorption rate constant, respectively, K_d (g·mg^{-1}min$^{-1/2}$) is the rate constant of intraparticle diffusion, and I is a parameter related to the thickness of the boundary layer.

To further analyze the adsorption mechanism of BN, Freundlich and Langmuir fit the thermodynamic data. The linearization formulas of the two fits are as follows:

Freundlich model:

$$lnq_e = lnK_F + nlnC_e \quad \ldots(7)$$

Langmuir model:

$$\frac{1}{q_e} = \frac{1}{q_m} + \frac{1}{K_L \times q_m} \cdot \frac{1}{C_e} \quad \ldots(8)$$

Characterization Methods

In this study, the JEM-1011 transmission electron microscope of Japan Electronics Company was used for TEM characterization to analyze the fine internal structure of materials, and the scanning electron microscope (SEM) of Japan Electronics (JEOL) and JSM-6360LV was used to analyze the surface topography of materials. This team used the Fourier infrared spectrometer (NICOLET6700) of the United States Thermoelectric Technology Company to determine BN samples' molecular structure and chemical composition, ranging from 400 to 4000 cm-1. The resolution is better than 4 cm$^{-1.}$ At the same time, an X-ray energy spectrometer (XRD), manufactured in Panalytical, Netherlands, model Empyrean, uses a *Cu* target as the radiation source. XRD is mainly used in this paper to determine the crystal shape of BN material.

RESULTS AND DISCUSSION

Adsorption Results

pH has a significant effect on the adsorption of La(III) by BN, and it can be seen from Fig. 1(A) that the adsorption effect of BN on La(III) increases significantly with the increase of pH. However, it can be found from Fig. 1(B) that after the pH value exceeds 6.0, the residual concentration of

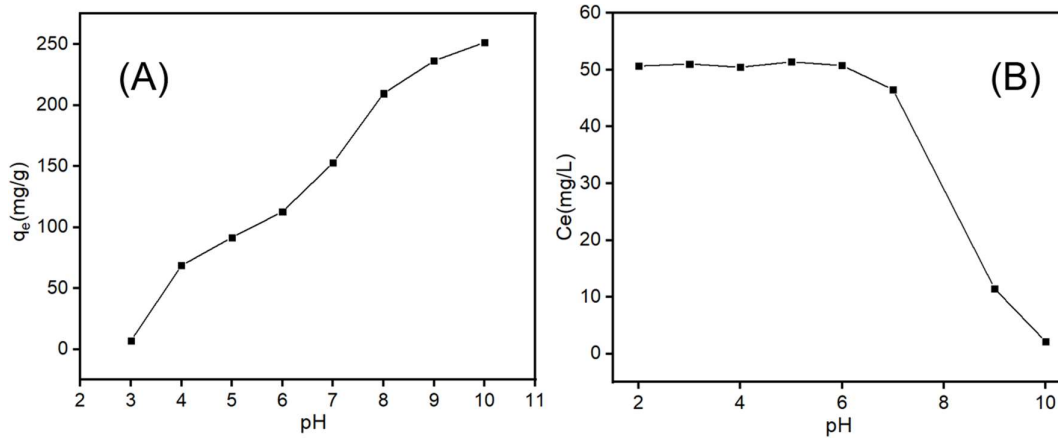

Fig. 1: (A) Effect of Initial pH on La(III) Adsorption by BN (q_e), (B) Under different pH conditions, the residual concentration of La(III) solution after sufficient reaction (C_e). Experimental conditions, C = 50 mg·L^{-1}, m = 20 mg, V = 100 mL

La(III) solution will gradually decrease even if no adsorbent is added. This is because La(III) will precipitate at a higher pH, thus affecting the experimental results. Therefore, considering both, pH 6.0 or 7.0 is selected for the subsequent experiments.

To explore the influence of the amount of adsorbent on the adsorption performance, different qualities of adsorbent were added into the lanthanum solution of 100 mL and 50 mg·L^{-1}, showing that the amount of adsorbent is closely related to the adsorption performance. Increasing the amount of adsorbent will lead to a gradual decrease in the adsorption amount of adsorbent, but the removal rate of La(III) will gradually increase.

As can be seen from Fig. 3 (A), the concentration also significantly impacts the performance of the adsorbent. With

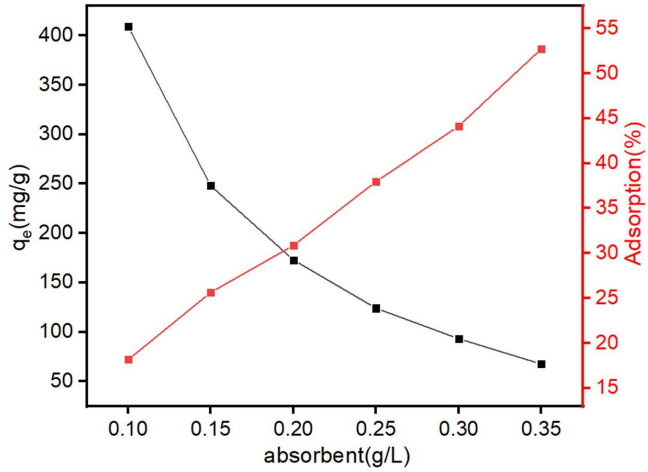

Fig. 2: Effects of different adsorbent concentrations on BN adsorption capacity (q_e) and removal rate.

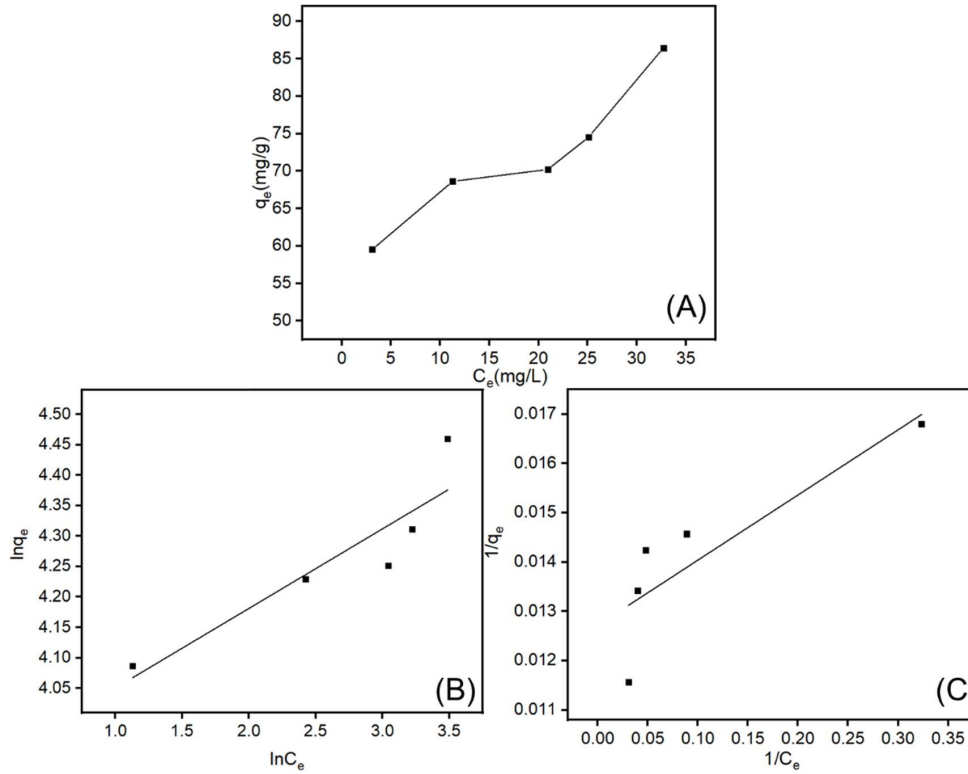

Fig. 3: (A) Isotherm of La(III) Adsorption on BN, (B) Freundlich model, (C) Langmuir model.

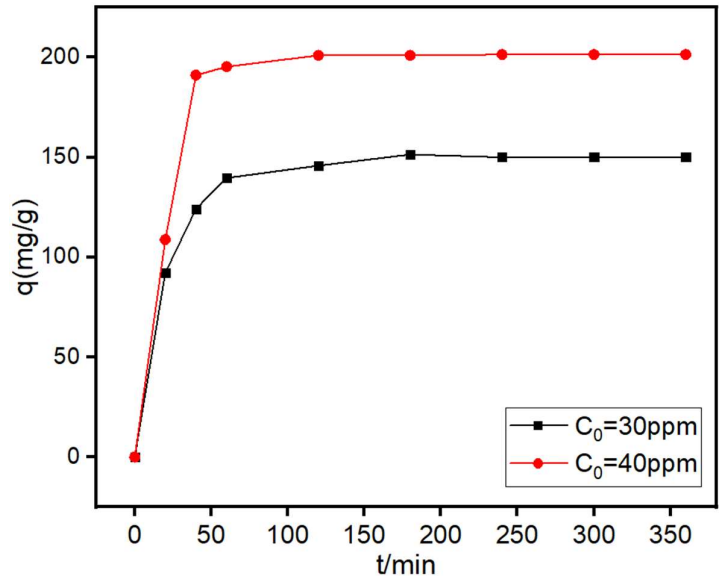

Fig. 4: The adsorption time curve of BN to 30 mg·L^{-1} and 40 mg·L^{-1} La(III) Experimental solution conditions, V = 100 mL, m = 20 mg, pH = 7.0

the increase of the concentration, the adsorption capacity of the adsorbent also increases. To explore its adsorption mechanism, we performed Freundlich and Langmuir fitting on the curve. The results in Fig. 3 (B-C) show that the experimental data are not in line with the Langmuir fitting model and the Freundlich fitting model, indicating that the adsorption mechanism is relatively complex, with both single-layer adsorption and multi-layer adsorption.

Next, the kinetic curve of BN adsorption of La(III) solution is discussed. Fig. 4 shows that no matter La(III), the initial concentration of solution is 30.0 mg·L^{-1} or 40.0 mg·L^{-1}, the growth trend of BN adsorption capacity is roughly similar. With the increase of time, the adsorption capacity increases gradually. The adsorption capacity increased rapidly, the growth was relatively slow in 60~180 min, and the adsorption equilibrium was reached around 180 min. When the initial concentration of La(III) solution is 30.0 mg·L^{-1}, the maximum adsorption capacity of BN on La(III) is 150.05 mg·g^{-1}. When the concentration is 40.0 mg·L^{-1}, the maximum adsorption capacity reaches 201.46 mg·g^{-1}. The results are consistent with the previous results of the effect of concentration on the adsorbent, indicating that the experimental results have good reproducibility.

Fig. 5 (A) is a pseudo-first-order model fitting of the kinetic curve of BN adsorption La(III) solution, Fig. 5 (B) is a pseudo-second-order fitting model, and Fig. 5 (C) is an Elovich model fitting combined. After fitting and analysis, it is found that the kinetic curve of BN to La(III) solution is more in line with the pseudo-second-order fitting model, indicating that the adsorption process is mainly chemical adsorption (Li et al. 2020a). Although the adsorption of BN can be obtained by fitting the pseudo-first-order and pseudo-second-order models, the adsorption mechanism cannot be further speculated. Therefore, using the particle internal diffusion model, as shown in Fig. 5 (D), the adsorption process is divided into two stages. The first stage La(III), diffuses to the surface of the material to complete the adsorption, and the second stage adsorption reaches the adsorption equilibrium (Shan et al. 2020).

Characterization Results

SEM and TEM characterize the BN material to analyze its surface morphology and internal structure. The results are shown in Fig. 6. According to SEM images (A), (B), and TEM images (C), BN material presents a circular or elliptical sheet structure with an average diameter ranging from one micron to several microns. The sheet structure can increase the contact area and increase adsorption efficiency.

The material's microstructure will have a greater impact on the macro performance, and the functional group will significantly impact the adsorption process. Therefore, we conducted the infrared spectroscopic measurement and characterization of the prepared BN material. It can be seen from Fig. 7 (A) that there are two characteristic absorption peaks at ~1380cm^{-1} and ~810cm^{-1}, which are caused by the bending vibration of B-N-B and B-N combined by the sp^2 bond. In contrast, a wide peak appeared at ~3420cm^{-1}, which was attributed to the fact that BN material may contain more -OH groups and have a strong vibration peak here (Zhang et al. 2021, Hou et al. 2019). The absorption peak at ~1592

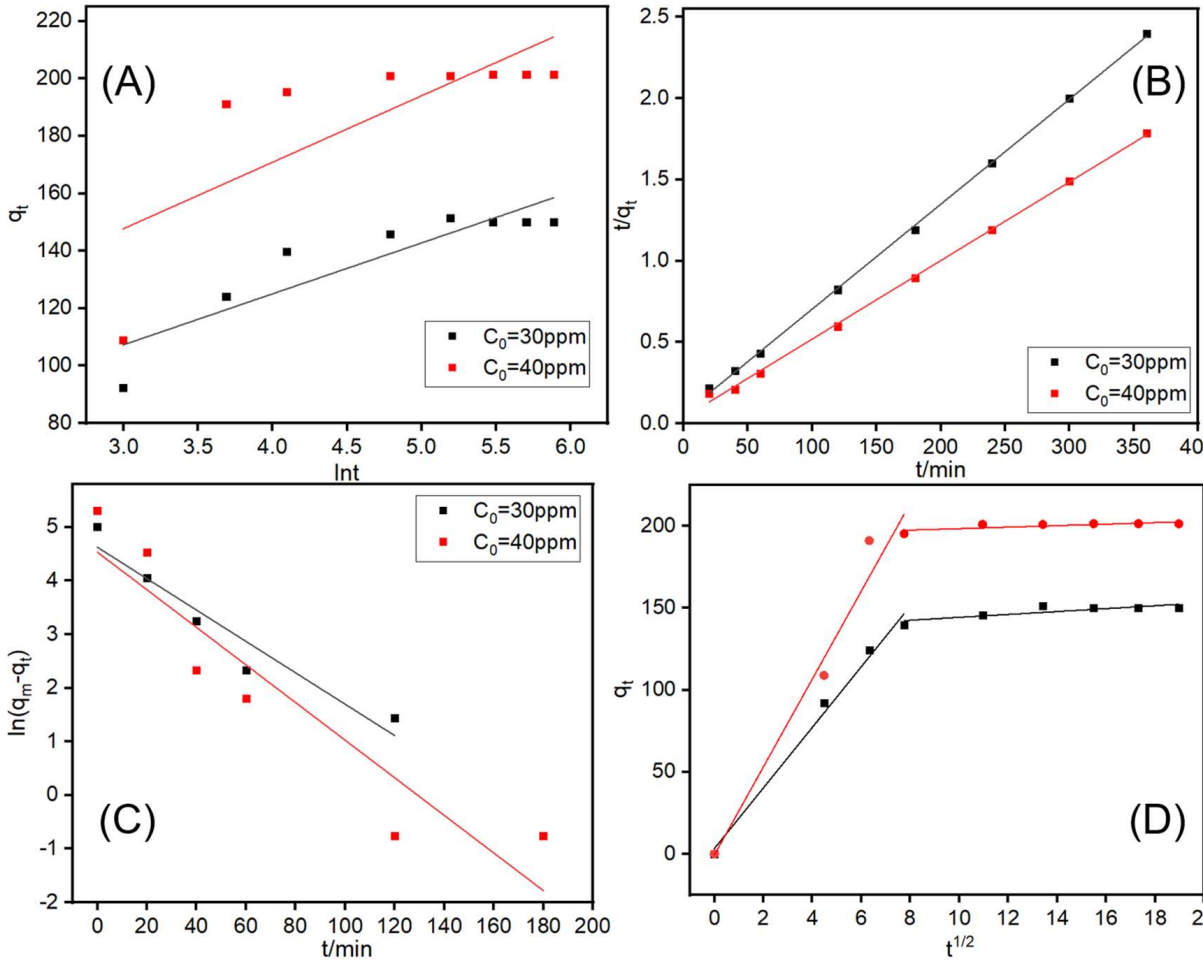

Fig. 5: (A) pseudo-first-order model; (B) pseudo-second-order model; (C) Elovich model; (D) intra-particle diffusion model.

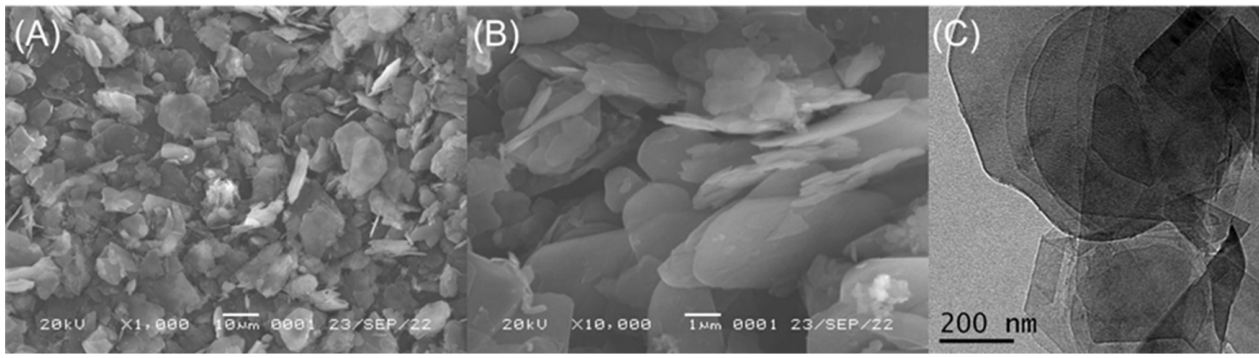

Fig. 6: (A, B) SEM image of the BN, (C) a TEM image of the BN.

cm^{-1} can be attributed to the uneven surface of BN material, which changes the position of the acromion of the B-N bond (Tang et al. 2008).

To determine the crystal plane of the material, we conducted XRD characterization of the material. Fig. 7 (B) is the XRD characterization image of BN. The front appearing at 26.7°, 41.5°, and 55° corresponds to the crystal planes (002), (100), and (004) of BN, respectively, which is similar to the results of Li et al. (2015) and Fu et al. (2023).

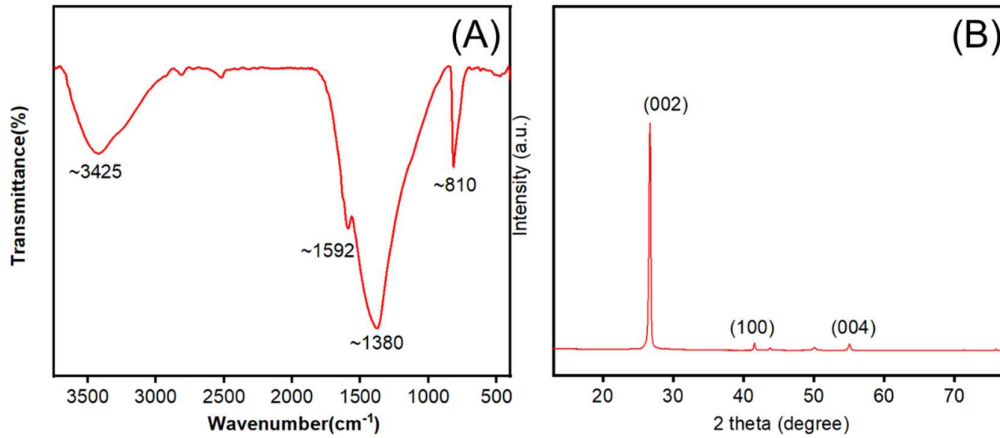

Fig. 7: (A) FT-IR spectrum of BN (B) XRD pattern of BN.

CONCLUSION

Based on the above experiments and analysis, this paper describes a preparation method of BN material and explores the adsorption performance and mechanism of BN for La(III) solution. The results show that BN has a good adsorption effect on La(III) in water, and the adsorption property of the material is closely related to the concentration of a solution with the amount of adsorbent, pH value, and contact time.

Under 303K and pH = 7.0, the maximum adsorption capacity of BN can reach 201.45mg·g^{-1}. The results show that the kinetic fitting of the adsorption experiment conforms to the pseudo-second-order model fitting, indicating that the adsorption experiment is chemical adsorption. The in-particle diffusion model shows that the adsorption process is mainly divided into two stages: La(III) diffusion to BN surface stage, and the adsorption reaches the adsorption equilibrium stage.

Through SEM, TEM, FT-IR, and XRD characterization, it is found that the BN prepared by this method is very similar to the common BN materials in the structure, which proves that the preparation of BN by this method is feasible. The preparation method has a low cost, simple process, and good adsorption effect on La(III), which has a good application prospect in water pollution control.

ACKNOWLEDGEMENT

The work was supported by the Zhejiang Basic Public Welfare Research project in the 2018 year (LGG18B070002) and the Project of Shaoxing University (No. 2022LG003). We also sincerely thank the young and middle-aged academic cadres from Shaoxing University.

REFERENCES

Chen, Z.Y. and Zhu, X. D. 2008. Accumulation of rare earth elements in bone and its toxicity and potential hazard to health. J. Ecol. Rural. Environ., 24: 88-91.

Cheng, J., Cheng, Z., Hu, R., Cui, Y., Cai, J., Li, N. and Hong, F. 2014. Immune dysfunction and liver damage of mice following exposure to lanthanoids. Environ. Toxicol., 29(1): 64-73.

Du, Y., Wu, Q., Kong, D., Shi, Y., Huang, X., Luo, D. and Leung, J.Y. 2020. Accumulation and translocation of heavy metals in water hyacinth: Maximising green resources to remediate sites impacted by e-waste recycling activities. Ecol. Indic., 115: 106384.

Fu, C.K., He, Y.C., Yang, C.Y., He, J.Y. and Wang, L.X. 2023. Investigation of Adsorption of Nd (III) on Boron Nitride Nanosheets in Water. Nat. Environ. Pollut. Technol., 16: 225-233

Hou, Y., Yang, W., Zhong, C., Wu, S., Wu, Y., Liu, F. and Wen, G. 2019. Thermostable SiCO@ BN sheets with enhanced electromagnetic wave absorption. Chem. Eng. J., 378: 122239.

Kusrini, E., Wicaksono, W., Gunawan, C., Daud, N. Z. A. and Usman, A. 2018. Kinetics, mechanism, and thermodynamics of lanthanum adsorption on pectin extracted from durian rind. J. Environ. Chem. Eng., 6(5): 6580-6588.

Lale, A., Bernard, S. and Demirci, U. B. 2018. Boron nitride for hydrogen storage. ChemPlusChem, 83(10): 893-903.

Li, J., Huang, Y., Liu, Z., Zhang, J., Liu, X., Luo, H. and Tang, C. 2015. Chemical activation of boron nitride fibers for improved cationic dye removal performance. J. Mater. Chem. A, 3(15): 8185-8193.

Li, J., Xiao, X., Xu, X., Lin, J., Huang, Y., Xue, Y. and Tang, C. 2013. Activated boron nitride is an effective adsorbent for metal ions and organic pollutants. Sci. Rep., 3(1): 1-7.

Li, L., Chang, K., Fang, P., Du, K., Chen, C., Zhou, S. and Guo, X. 2020b. Highly efficient scavenging of Ni (II) by porous hexagonal boron nitride: kinetics, thermodynamics, and mechanism aspects. Appl. Surf. Sci., 521: 146373.

Li, L., Guo, X., Jin, Y., Chen, C., Abdullah M.A., Marwani, H.M. and Sheng, G. 2020a. Distinguished Cd (II) capture with rapid and superior ability using porous hexagonal boron nitride: Kinetic and thermodynamic aspects. Inorg. Mater., 35(3): 461-475.

Liu, F., Li, S., Yu, D., Su, Y., Shao, N. and Zhang, Z. 2018. Template-free synthesis of oxygen-doped bundlelike porous boron nitride for highly efficient removal of heavy metals from wastewater. ACS Sustain. Chem. Eng., 6(12): 16011-16020.

Liu, J., Li, N., Ma, L., Duan, Y., Wang, J., Zhao, X. and Hong, F. 2010. Oxidative injury in the mouse spleen caused by lanthanides. J. Alloys Compd., 489(2): 708-713.

Sert, Ş., Kütahyali, C., İnan, S., Talip, Z., Çetinkaya, B. and Eral, M. 2008. Biosorption of lanthanum and cerium from aqueous solutions by Platanus orientalis leaf powder. Hydrometallurgy, 90(1): 13-18.

Shan, R., Shi, Y., Gu, J., Bi, J., Yuan, H., Luo, B. and Chen, Y. 2020. Aqueous Cr (VI) removal by biochar derived from waste mangosteen shells: Role of pyrolysis and modification on its absorption process. J. Environ. Chem. Eng., 8(4): 103885.

Shen, Y., Zhang, S., Li, S., Xu, X., Jia, Y. and Gong, G. 2014. Eucalyptus tolerance mechanisms to lanthanum and cerium: subcellular distribution, antioxidant system, and thiol pools. Chemosphere, 117: 567-574.

Shin, S.H., Kim, H.O. and Rim, K. 2019. Worker safety in the rare earth elements recycling process from the review of toxicity and issues. Saf. Health Work, 10(4): 409-419.

Tang, C., Bando, Y., Huang, Y., Zhi, C. and Golberg, D. 2008. Synthetic routes and formation mechanisms of spherical boron nitride nanoparticles. Adv. Funct. Mater., 18(22): 3653-3661.

Wang, D., Luo, W., Zhu, J., Wang, T., Gong, Z. and Fan, M. 2021. Potential of removing Pb, Cd, and Cu from aqueous solutions using a novel modified ginkgo leaves biochar by simply one-step pyrolysis. Biomass Convers. Biorefin., 2: 1-10.

Wu, D., Zhang, L., Wang, L., Zhu, B. and Fan, L. 2011. Adsorption of lanthanum by magnetic alginate□chitosan gel beads. J. Chem. Technol. Biotechnol., 86(3): 345-352.

Wu, F.C., Tseng, R.L. and Juang, R.S. 2009. Characteristics of Elovich equation used to analyze adsorption kinetics in dye-chitosan systems. Chem. Eng. J., 150(2-3): 366-373.

Wu, H., Zhang, X., Li, X., Wu, Y. and Pei, F. 2005. Acute biochemical effects of La $(NO_3)_3$ on liver and kidney tissues by magic-angle spinning 1H nuclear magnetic resonance spectroscopy and pattern recognition. Anal. Biochem., 339(2): 242-248.

Zarros, A., Byrne, A.M., Boomkamp, S.D., Tsakiris, S. and Baillie, G.S. 2013. Lanthanum-induced neurotoxicity: solving the riddle of its involvement in cognitive impairment. Arch. Toxicol., 87: 2031-2035.

Zhang, Y., Si, H., Liu, S., Jiang, Z., Zhang, J. and Gong, C. 2021. Facile synthesis of BN/Ni nanocomposites for effective regulation of microwave absorption performance. J. Alloys Compd., 850: 156680.

Zhen, H.B., Xu, Q., Hu, Y.Y. and Cheng, J.H. 2012. Characteristics of heavy metals capturing agent dithiocarbamate (DTC) for treatment of ethylene diamine tetraacetic acid–Cu (EDTA–Cu) contaminated wastewater. Chem. Eng. J., 209: 547-557.

Zhi, C., Bando, Y., Tang, C. and Golberg, D. 2010. Boron nitride nanotubes. Mater. Sci. Eng. R Rep., 70(3-6): 92-111.